Supporting information:

The distinctive phase stability and defect physics in $CsPbI_2Br$ perovskite

Yuxuan Chen,[†] *Tingting Shi,*[*‡] *Pengyi Liu,*[‡] *Weiguang Xie,*[‡] *Ke Chen,*[‡] *Xin Xu,*[‡] *Lingling Shui,*[†] *Chaoqun Shang,*[†] *Zhihong Chen,*[§] *Hin-Lap Yip,*[*□] *and Guofu Zhou,*[†] *Xin Wang,*[*†]

[†] National Center for International Research on Green Optoelectronics, South China Normal University, Guangzhou 510006, China

[‡] Siyuan Laboratory, Guangzhou Key Laboratory of Vacuum Coating Technologies and New Energy Materials, Guangdong Provincial Engineering Technology Research Center of Vacuum Coating Technologies and New Energy Materials, Department of Physics, Jinan University, Guangzhou 510632, China

[□] State Key Laboratory of Luminescent Materials and Devices, Institute of Polymer Optoelectronics Materials and Devices, School of Material Science and Engineering, South China University of Technology, Guangzhou 510640, China

[§] Key Laboratory for Water Quality and Conservation of the Pearl River Delta, Ministry of Education, Institute of Environmental Research at Greater Bay, Guangzhou University, Guangzhou, 510006, China

Corresponding Author

*E-mail: ttshi@email.jnu.edu.cn

*E-mail: wangxin@scnu.edu.cn

*E-mail: msangusyip@scut.edu.cn

COMPUTATIONAL METHODS

All calculations were performed using the density functional theory (DFT), as implemented in the Vienna *Ab initio* Simulation Package (VASP)[1,2] with the projector augment wave (PAW)[3] method. The exchange and correlation potential was described with the Perdew-Burke-Ernzerhof (PBE) of the generalized gradient approximation (GGA).[37] The cutoff energy for basis functions was 400 eV and the energy and force on each ion were reduced below 10^{-4} eV/atom and 0.05 eV/Å. In the study, a more accurate Heyd-Scuseria-Ernzerhof (HSE06) hybrid functional[6] with a screening parameter μ 0.2 $Å^{-1}$ was also employed. Moreover, it is well-known that the spin-orbit coupling (SOC) effect in $CsPbX_3$(X=I, Br or Cl) has great effect on the calculated band gap. In order to check the effect of the SOC, SOC effect was considered in our calculations. A 3×3×3 supercell (α-phase $CsPbI_2Br$, containing 135 atoms) and a 2×2×3 supercell (β-phase $CsPbI_2Br$, containing 120 atoms) were used for the defect calculations, and the Brillouin zone was sampled by the Γ point with k-spacing of 0.2 $Å^{-1}$. The defect properties were only calculated by using GGA(PBE) method, because the use of a large supercell is expensive computational time by using HSE06 method. All calculations were performed at 0 K and 0 GPa, without taking into account the effect of zero-point motion. The high-symmetry special points in the first Brillouin zone were used in band structure calculations: X (0.0, 0.5, 0.0), R (0.5, 0.5, 0.5), M (0.5, 0.5, 0.0), and Γ (0.0, 0.0, 0.0) for α-phase $CsPbI_2Br$; R (0.5, 0.5, 0.5), X (0.0, 5.0, 0.0), Z (0.0, 0.0, 0.5), Γ (0.0, 0.0, 0.0), A (0.5, 0.5, 0.5) and M (0.5, 0.5, 0.0) for β-phase $CsPbI_2Br$.

The formation energy $\Delta H_{D,q}(E_f, \mu)$ for a defect α at charge state q can be calculated using the supercell model as defined,[7,8]

$$\Delta H_{\mathrm{D,q}}(E_F,\mu) = E(D,q) - E(\mathrm{host}) + q\left(E_{\mathrm{V}} + E_F\right) - \sum n_\alpha \mu_\alpha \quad (1)$$

Where E(D, q) is the total energy of the supercell containing the defect, and E(host) is the total energy of the same supercell with the absence of defect; E_V is the valence-band maximum (VBM) energy of the host material and E_F is the Fermi level referred to the VBM; n_α is the number of atom α that have been added to (n_α>0) or removed from (n_α<0) the supercell, and q is the number of electrons, transferred from the supercell to the reservoirs in forming the defect cell; μ_α is the chemical potential of the α atom, which can be expressed with respect to that of the elemental phase (μ_α^{el}) by $\mu_\alpha = \mu_\alpha^{el} + \Delta\mu_\alpha$. The μ_α value varies depending on the experimental conditions.

The allowed μ_α values and chemical potential window of the $CsPbI_2Br$ is determined using three steps. First, to stabilize the $CsPbI_2Br$ phase, the following thermodynamic equilibrium must be reached:

$$\Delta\mu_{Cs} + \Delta\mu_{Pb} + 2\Delta\mu_I + \Delta\mu_{Br} = \Delta H\,(CsPbI_2Br) = -7.40\ \mathrm{eV} \quad (2)$$

Where ΔH ($CsPbI_2Br$) is the formation enthalpy of $CsPbI_2Br$, as referred to the elemental solids Cs (cubic, space group *Fm3m)*, Pb (cubic, *Fm−3m*), I (orthorhombic, *Immm*), and Br (orthorhombic, *Pnma*). Second, to exclude the elemental phases, it is required that $\Delta\mu_{Cs} < 0$, $\Delta\mu_{Pb} < 0$, $\Delta\mu_I < 0$ and $\Delta\mu_{Br} < 0$. Third, to avoid the formation of the competing secondary phases including binary compounds CsI (cubic, *Fm−3m*), PbI_2 (hexagonal, *P3m1*) and $PbBr_2$ (tetragonal, P42/mnm) ; and ternary compounds $CsPbI_3$ (tetragonal, *P4/mbm*, simulated from β-$CsSnI_3$[9,10]), the following equations also must be satisfied:

$$\triangle\mu_{Cs} + \triangle\mu_I < \triangle H\,(CsI) = -5.51\mathrm{eV} \quad (3)$$

$$\triangle\mu_{Pb} + 2\triangle\mu_I < \triangle H\,(PbI_2) = -8.64\ \mathrm{eV} \quad (4)$$

$$\triangle\mu_{Pb} + 2\triangle\mu_{Br} < \triangle H\,(PbBr_2) = -9.60\ eV \quad (5)$$

$$\triangle\mu_{Cs} + \triangle\mu_{Pb} + 3\triangle\mu_{I} < \triangle H\,(CsPbI_3) = -14.15\ eV \quad (6)$$

Under the above constraints, the allowed $\triangle\mu_{Cs}$, $\triangle\mu_{I}$, and $\triangle\mu_{Br}$ for β-phase $CsPbI_2Br$ are bound in a polyhedron as shown in Fig. 4, whereas $\triangle\mu_{Cs}$ is associated with $\Delta\mu_{Pb}$, $\Delta\mu_{I}$ and $\Delta\mu_{Br}$ through equation (2). It is worth noting that the competing ternary compounds $CsPbI_3$ cannot formed, which may due to its relatively high decomposition energy compared with $CsPbI_2Br$.

The defect charge-transition energy level $\varepsilon_\alpha(q/q')$ corresponds to the E_F at which the formation energy $\Delta H(\alpha, q) = \Delta H(\alpha, q')$ for a defect α with different charge state q and q′, and can be described as,

$$\varepsilon_\alpha(q/q') = \left[\Delta E(\alpha,q) - \Delta E(\alpha,q')\right]/(q'-q) \quad (7)$$

To explore the optical properties of $CsPbI_2Br$, the optical absorption spectra are simulated by converting the complex dielectric function to the absorption coefficient α_{abs} according to the following formula,[11]

$$\alpha_{abs} = \sqrt{2}\omega\left(\sqrt{\varepsilon_1^{\,2}(\omega) + \varepsilon_2^{\,2}(\omega)} - \varepsilon_1(\omega)\right)^{\frac{1}{2}} \quad (8)$$

where $\varepsilon_1(\omega)$ and $\varepsilon_2(\omega)$ are the real and imaginary parts, respectively, of the frequency dependent complex dielectric function $\varepsilon(\omega)$. Taking into account the tensor nature of the dielectric function, $\varepsilon_1(\omega)$ and $\varepsilon_2(\omega)$ are averaged over three polarization vectors (along x, y, and z directions).

All structures are taken from Materials Project Website (https://materialsproject.org/).[12]

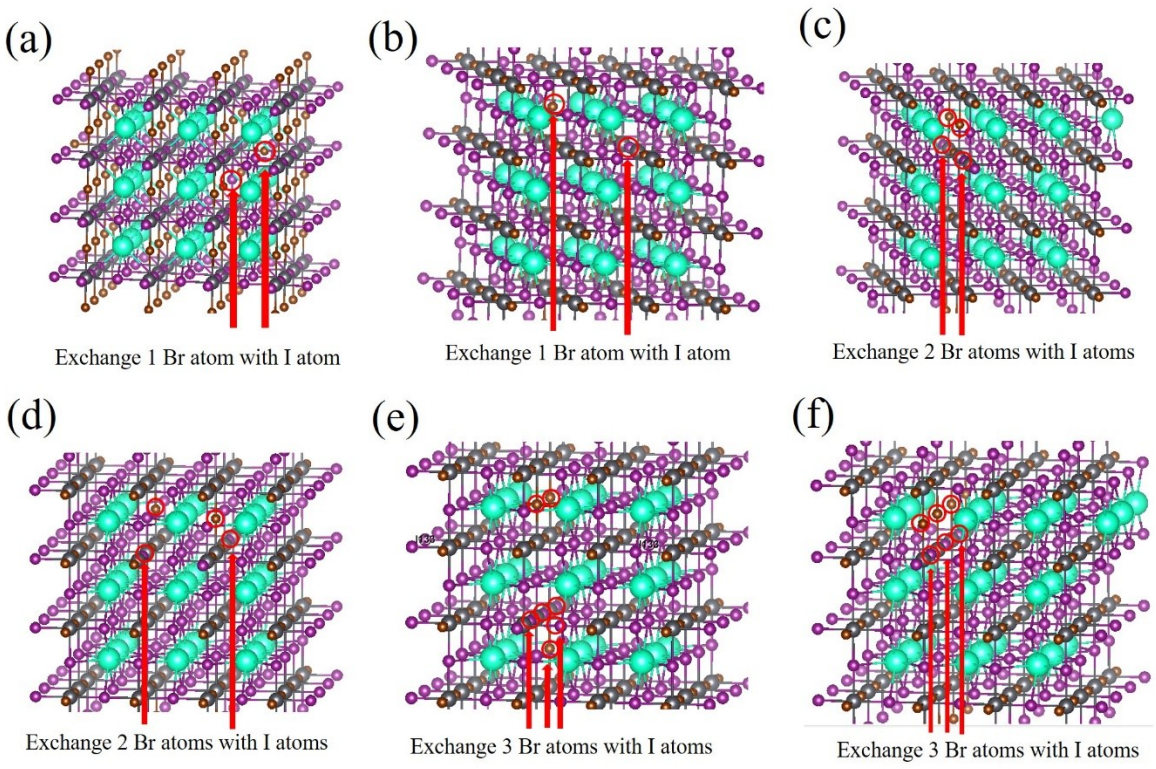

Fig. S1. The relaxed crystal structures for six representational configurations selected compositions of the 3×3×3 supercell α-$CsPbI_2Br$. Disorder Br and I compositions are presented in panels (a), (b), (c), (d), (e) and (f), respectively, the exchanged atoms are marked in red circles. The green, black, purple and brown balls denote Cs, Pb, I and Br atoms, respectively.

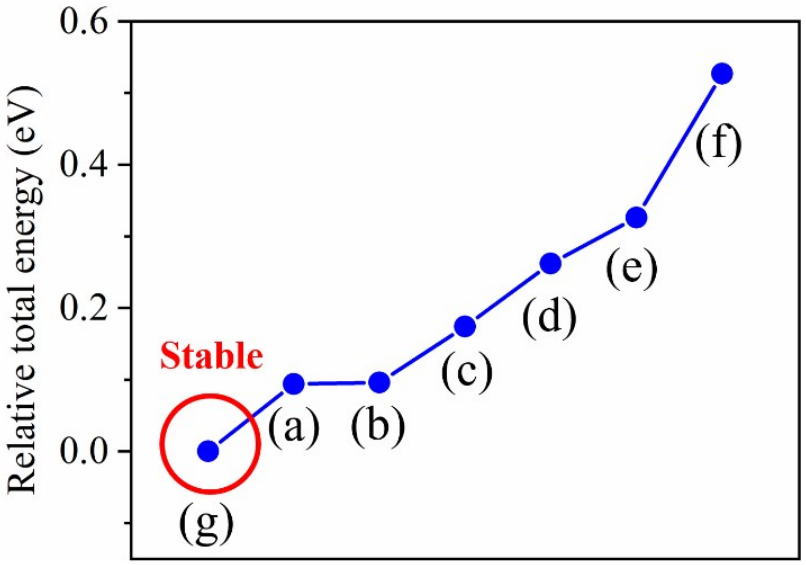

Fig. S2. Relative total energy for six representational configurations selected compositions in **Fig. S1** compared with periodically alternating arrangement prefect 3×3×3 supercell α-$CsPbI_2Br$ (denoted as panels (g)).

We chose six representational configurations selected compositions with different Br-I occupation sites and calculated the total energy by using GGA-PBE method. The results indicate that the periodically alternating arrangement is the most stable structure, therefore, the defect structures were set based on this structure.

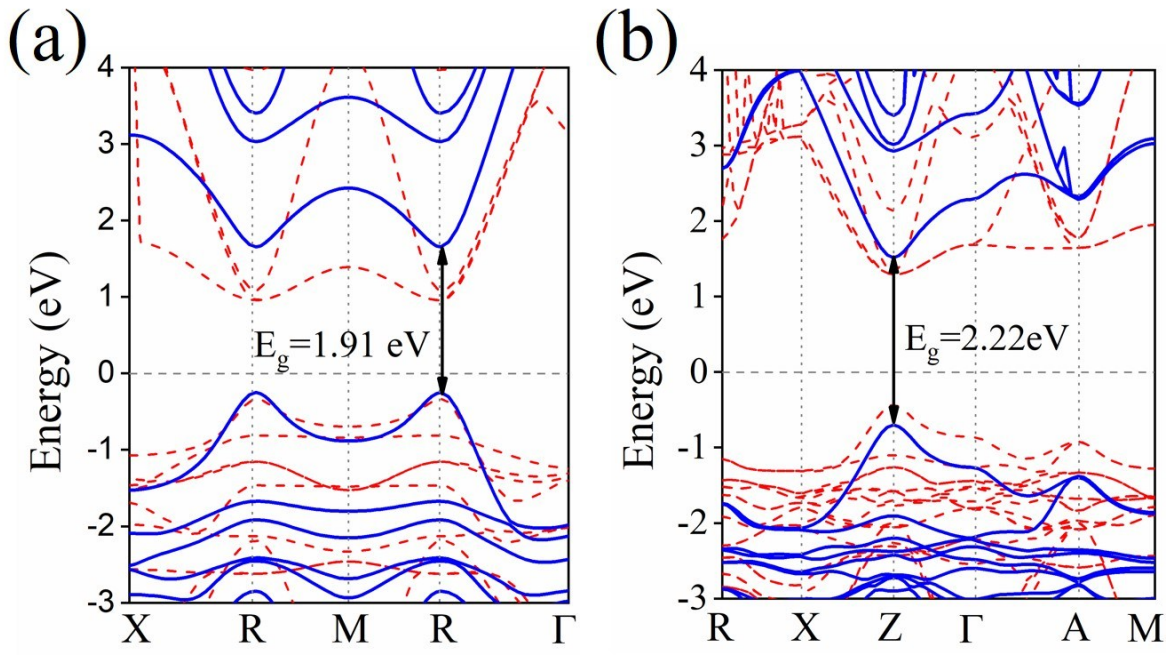

Fig. S3. Calculated band structures using GGA (red dashed line) and HSE06+SOC (blue solid line) method: (a) α-$CsPbI_2Br$ (d) β-$CsPbI_2Br$, respectively. The Fermi level is set to be 0 eV and denoted as a black dashed line.

Table S1. Total energy calculations of $CsPbI_2Br$ (3×3×4 supercell, containing 180 atoms for α-phase; 3×3×2 supercell for, containing 180 atoms) and $CsPbI_2Br$ with V-Pb defect (179 atoms) by using GGA-PBE method

	Total energy (eV)	**Energy/per atom (eV)**
α-phase V-Pb	-524.50054	-2.930
Pure-α-phase	-531.51589	-2.952
β-phase V-Pb	-542.13122	-3.012
Pure β-phase	-547.90836	-3.011

From this table, we can see that the total energy of Pure β-phase $CsPbI_2Br$ is slightly (59 meV/per atom) smaller than that of α-phase, and the total energy of β-phase V-Pb is slightly (19 meV/per atom) smaller than that of α-phase, indicating that β-phase $CsPbI_2Br$ is more stable than α-phase.

Table S2. Summary of the calculated band gaps of $CsPbI_2Br$ with different methods

	Cubic (eV)	**Tetragonal (eV)**
PBE	1.49	1.74
PBE+SOC	0.18	0.63
25%HSE06	1.94	2.30
63%HSE06+SOC	1.91	2.22
G_0W_0	2.82	3.08

*Experimental band gap 1.91 eV [13,14]

Table S3. Calculated formation energies (in eV) for neutral defects in β-$CsPbI_2Br$ at chemical potential points A and D shown in Fig. 4. For acceptor defects, their formation energies are at the VBM, while for donor defects, their formation energies are at the CBM.

	V-Cs	V-Pb	I_{Pb}	I_{Cs}	Br_{Cs}	Br_{Pb}	Br_i	I_i	Cs_{Pb}
A	1.44	2.13	3.68	1.61	3.94	3.93	0.72	0.92	1.58
D	0.35	-0.04	0.40	0.52	1.76	0.66	-0.37	-0.17	0.50

	V-Br	V-I	Pb_{Cs}	Pb_i	Cs_i	Cs_{Br}	Cs_I	Pb_I	Pb_{Br}
A	0.03	0.07	1.11	1.90	0.28	1.60	1.52	1.06	2.15
D	1.11	1.16	2.21	4.08	1.37	3.79	3.70	4.32	5.19

REFERENCES:

1 G. Kresse and J. Furthmiiller, *Comput. Mater. Sci.*, 1996, **6**, 15–50.

2 G. Kresse and J. Furthmu, *Phys. Rev. B*, 1996, **54**, 11169–11186.

3 D. Joubert, *Phys. Rev. B - Condens. Matter Mater. Phys.*, 1999, **59**, 1758–1775.

4 M. Ernzerhof and G. E. Scuseria, *J. Chem. Phys.*, 1999, **110**, 5029–5036.

5 J. P. Perdew, K. Burke and M. Ernzerhof, *Phys. Rev. Lett.*, 1996, **77**, 3865–3868.

6 J. Heyd, G. E. Scuseria and M. Ernzerhof, *J. Chem. Phys.*, 2003, **118**, 8207–8215.

7 C. G. Van De Walle and J. Neugebauer, *J. Appl. Phys.*, 2004, **95**, 3851–3879.

8 S. Lany and A. Zunger, *Phys. Rev. B - Condens. Matter Mater. Phys.*, 2008, **78**, 17–20.

9 I. Chung, J. H. Song, J. Im, J. Androulakis, C. D. Malliakas, H. Li, A. J. Freeman, J. T. Kenney and M. G. Kanatzidis, *J. Am. Chem. Soc.*, 2012, **134**, 8579–8587.

10 R. J. Sutton, M. R. Filip, A. A. Haghighirad, N. Sakai, B. Wenger, F. Giustino and H. J. Snaith, *ACS Energy Lett.*, 2018, **3**, 1787–1794.

11 S. Saha, T. Sinha and A. Mookerjee, *Phys. Rev. B*, 2000, **62**, 8828–8834.

12 A. Jain, S. P. Ong, G. Hautier, W. Chen, W. D. Richards, S. Dacek, S. Cholia, D. Gunter, D. Skinner, G. Ceder and K. A. Persson, *APL Mater.*, 2013, **1**, 011002.

13 G. Yin, H. Zhao, H. Jiang, S. Yuan, T. Niu, K. Zhao, Z. Liu and S. (Frank) Liu, *Adv. Funct. Mater.*, 2018, **28**, 1803269.

14 W. Chen, H. Chen, G. Xu, R. Xue, W. Chen, H. Chen, G. Xu, R. Xue, S. Wang and Y. Li, *Joule*, 2019, **3**, 191–204.